CrystEngComm

Accepted Manuscript

This article can be cited before page numbers have been issued, to do this please use: M. Vandichel, J. Hajek, A. Ghysels, A. De Vos, M. Waroquier and V. Van Speybroeck, *CrystEngComm*, 2016, DOI: 10.1039/C6CE01027J.

ROYAL SOCIETY OF CHEMISTRY

www.rsc.org/crystengcomm

View Article Online
DOI: 10.1039/C6CE01027J

CrystEngComm

ARTICLE

Water coordination and dehydration processes in defective UiO-66 type metal organic frameworks

Received 00th January 20xx,
Accepted 00th January 20xx

DOI: 10.1039/x0xx00000x

www.rsc.org/

M. Vandichel,[a*] J. Hajek, [a] A. Ghysels, [a] A. De Vos, [a] M. Waroquier, [a*] and V. Van Speybroeck [a]

The UiO-66 metal organic framework is one of the most stable thermally and chemically hybrid material reported to date. However it is also accepted that the material contains structurally embedded defects, which may be engineered to enhance properties towards specific applications such as catalysis, sensing,… The synthesis conditions determine to a large extent the level of perfection of the material and additionally the catalytic activity may be enhanced by a post-synthesis activation at high temperature in vacuum, in which defect coordinating species (H2O, HCl, monocarboxylic modulators, etc.) evaporate. The molecular level characterization of defects is extremely challenging both from theoretical as experimental point of view. Such experimental endeavor was recently proposed via experimental SXRD measurements, also unraveling the coordination of water on the Zr-O-Zr defect sites. [Angew. Chem. Int. Ed., 2015,54,11162-11167]. The present work provides a theoretical understanding of defect structures in the UiO-66(Zr) by means of periodic Density Functional Theory calculations and ab initio molecular dynamics simulations. A range of defect structures are generated with a different number of missing linkers. For each of the defects the free energetic and mechanical stability is discussed and the coordination of water and charge balancing hydroxide ions is studied. For catalysis applications the material is mostly pretreated to remove water by dehydration reactions. For each of the proposed defect structures mechanistic pathways for dehydration reactions of the Zr-bricks are determined employing Nudged Elastic Band (NEB) calculations. During the dehydroxylation trajectory loose hydroxyl groups and terephthalate decoordinations are observed. Furthermore dehydration reactions are lower activated if terephthalate linkers are missing in the immediate environment of the inorganic brick. The creation of defects and dehydration processes have a large impact on the mechanical properties of the material, which is evidenced by lower bulk moduli and elastic constants for structures with more defects.

Introduction

Metal-Organic Frameworks (MOFs) show a huge potential within catalysis given their high metal content and porosity to enable fast reactant and product diffusion from the reactive metal center [1-3]. Conceptually major advances have been made in the last decade to circumvent the structural lability and lack of active sites in coordinatively saturated framework materials. Currently materials have been synthesized with an outstanding thermal stability over a broad pH range and with active sites which may be engineered at the molecular level. [4] Originally, the catalytic activity of MOFs was attributed to the presence of structural, coordinatively unsaturated active sites [5-7]. The active sites should be freely accessible to reagent molecules, preferably via large channels and cavities. Later, MOFs with apparently fully saturated and thus inaccessible metal sites were also found to be catalytically active[8-10] and missing terephthalate linkers (structural defects) were postulated to be responsible for the catalytic activity. Theory succeeded also in explaining the observed catalytic activity in these materials by means of quantum chemical DFT calculations[8-13] on defective cluster models. It should be noted that already in 2008, it has been suggested that structural defects lie on the basis of an increased catalytic activity. Farrusseng and co-workers[14] succeeded in engineering structural defects in coordinatively unsaturated materials. They used monocarboxylate synthesis modulators to create more linker defects in MOF-5, leading to an enhanced catalytic activity[15]. Nowadays, the scientific community is completely aware of the importance of all kinds of defects in MOFs. A prototype example for such defect engineering is the UiO-66 material [10, 16-18], which was first synthesized by Lillerud et al. in 2008. [19] A lot of review and perspective papers are currently featuring this topic [20-23].

The defect-free UiO-66 is composed of inorganic $[Zr_6O_4(OH)_4]^{12+}$ bricks and terephthalate linkers (benzenedicarboxylate (BDC)) forming a coordinatively saturated framework with eightfold coordination of Zr with oxygen atoms, and forms a thermally and

[a] Center for Molecular Modeling, Ghent University, Technologiepark 903, B-9052 Zwijnaarde, Belgium

† E-mail: Matthias.Vandichel@ugent.be, Michel.Waroquier@ugent.be

Electronic Supplementary Information (ESI) available: [details of any supplementary information available should be included here]. See DOI: 10.1039/x0xx00000x

View Article Online
DOI: 10.1039/C6CE01027J

chemically very stable framework (reported first by Lillerud and co-workers[19]). Later, the technique of synthesis modulation with trifluoroacetic acid (TFA) and hydrochloric acid (HCl) has led to more defective UiO-66 frameworks[14,13]. While benzenedicarboxylate (BDC) and $[Zr_6O_4(OH)_4]^{12+}$ are usually building up the framework at synthesis conditions, the incorporation of other Zr-O-Zr coordinating species (synthesis modulators or MDL such like TFA, H_2O or HCl) instead of these BDC-linkers might appear at high MDL:BDC ratios in the reaction mixture[18]. This has theoretically been confirmed [13] by the high free energies required for direct removal of BDC linkers and/or replacement of a BDC linker by one or more MDLs under synthesis conditions. In a classical UiO-66 synthesis containing only HCl and benzoic acid as synthesis modulators, Lillerud et al.[24] have experimentally demonstrated the appearance of Zr-O-Zr coordination at linker deficiency sites in as-synthesized samples. Characterization of defect sites is very challenging, as the type of a deficiency in UiO-66 can be very broad varying from a missing linker to a missing Zr brick [17] . Many experimental techniques are available but a unique determination of the nature of these defects on the molecular level remains a very difficult task to accomplish. Nevertheless, such experimental knowledge is imperative to understand the catalytic activity of these defective materials, their adsorption properties and their thermal and chemical stability.[25] By means of single crystal X-ray diffraction (SXRD), the presence of two hydroxyl group terminations and/or coordinating water molecules has been observed.[24] Moreover, Yaghi et al.[26] performed a similar (more detailed) study investigating the different stages of UiO-66 treatments, using large single crystals up to 300 μm in diameter, while the largest crystals in the SXRD study of Øien et al. [24] reached only 10 μm. In open air at room temperature, they postulated the presence of an extra hydroxide anion per defect site, bringing the total amount of defect coordinating water units on 3. Very recently a theoretical paper of Ling and Slater [27], who performed a first principle molecular dynamics approach to further unravel the coordination of water and the charge compensating hydroxide ion in case one linker is missing in the conventional unit cell with four Zr-bricks. Trickett el al. [26] suggested a structure where the charge balancing hydroxide ion is stabilized by a hydrogen bond with a neighboring μ^3-OH group of the UiO-66 material, whereas the two neighboring Zr atoms are capped with physisorbed water molecules. Ling and Slater find that this structure is energetically not the most stable configuration and that instead the hydroxide ion prefers a coordination to the Zr site whereas two water molecules are physisorbed to the oxo atom and the other Zr atom. Depending on the temperature and concentration of water molecules various proton jumps may occur that allow to dynamically alter the acidity of active sites in the material. Dehydration/rehydration processes in MOFs have recently also been investigated experimentally in the frame of single crystal to single crystal (SC-SC) transformations.[28-30] However, on the theoretical level no much activity is noticed. In the UiO-66 material under investigation in this work structural SC-SC transformations don't take place.

In this paper we thoroughly investigate a variety of defect structures – in total six - in the UiO-66 material with varying number of coordinations for the Zr atoms. For each defect, we aim to unravel the precise structure and composition of the defects. As in ref. [27] we give a detailed insight into the coordination of water and charge balancing hydroxide ions, applying various computational protocols. Such a study is complementary to the experimental work of Trickett et al. [26] and the theoretical work of Ling and Slater. For each of the defect structures, we aim to unravel the process of dehydration or water removal. To generate active materials for catalysis, a thermal activation step is used, during which extra accessible Zr-sites are created, resulting from the removal of Zr-O-Zr coordinating species (TFA, H_2O, HCl, etc.)[13, 18]. Apart from the removal of such defect coordinating species, thermal activation does also promote dehydration (or water removal) reactions from inorganic bricks. In an earlier paper by some of the presenting authors, we proposed a mechanistic pathway for the dehydroxylation process for a fully saturated inorganic brick ($[Zr_6O_4(OH)_4]^{12+}$),[13] however, the influence of defects on the dehydroxylation processes is yet unknown and it is very difficult to study this effect experimentally. Herein, the dehydroxylation process is studied for structures with a varying number of defects in different periodic models.

It may be anticipated that introducing a large concentration of defects has also a large impact on the mechanical properties of the material. The mechanical behavior of UiO-66 type of materials received less attention so far. Recently Yot et al. [31] explored the mechanical behavior of UiO-66 by means of high-pressure powder X-Ray diffraction studies up to 3.5 GPa and it was observed that the material showed a gradual pressure-induced reversible decrease of crystallinity. The detailed effect of concentration of missing linkers was not explored so far by these authors. However the bulk modulus of the material was determined to be 17 GPa and by introducing amino functionalization this value could even be increased to 25 GPa. These values point towards a high mechanical robustness on top of their already well known thermal and chemical stabilities. From theoretical point of view, the bulk modulus of the defect free structure was reported to be 41 GPa by Wu et al. [25] using periodic DFT calculations. Herein we investigate for each of the proposed defect structures – six in total – the bulk modulus, to explore the influence of a varying number of linker deficiencies on the mechanical behaviour. We also explore the evolution of the bulk modulus during the dehydration pathways.

Overall this paper aims to add to a molecular level understanding of defect structures in the UIO-66 materials both in terms of nature of the defects, the coordination of water molecules, the removal of water molecules by means of dehydration reactions and the impact on the mechanical properties of the material.

Results and discussion

Before tackling the various items indicated in the Introduction, a periodic model representing the UiO-66 material with linker defects

View Article Online
DOI: 10.1039/C6CE01027J

needs to be constructed. Thereafter, this section will cover three main topics. First, the effect of linker defects on the stability of the structure and the mechanical properties of the material will be discussed. Second the coordination of water with the Zr-O-Zr defect created by removing one linker from a four bricks containing unit cell. Third, a systematical study of the dehydroxylation processes starting from different configurations of Zr-bricks representing the UiO-material with zero, one and two linker defects with computation of free energy barriers and reaction free energies.

A. Construction of periodic UiO-66 models with linker defects

From the crystallographic information file provided by Cavka et al.[19] containing a cubic unit cell with four inorganic $[Zr_6O_4(OH)_4]^{12+}$ bricks, an orthorhombic unit cell containing two inorganic bricks was constructed as displayed in **Figure 1**. For the energetic and mechanical characterization of the defects, this unit cell was chosen for the sake of computational efficiency. For the coordination of water we opted to consider the unit cell with four inorganic bricks. **Figure 1** also gives a good visualization of the relationship between these two unit cells. One missing linker in the smaller unit cell generates two missing linkers in the conventional unit cell and the identification of these linkers is facilitated by means of **Figure 1**. The further discussion deals with the smaller unit cell of two inorganic bricks, unless specified explicitly. Starting from the ideal defect free crystal structure A (unit cell formula: $<Zr_6O_4(OH)_4(RCOO)_{12}>_2$ in which $(RCOO^-)_2$ = BDC^{2-}) and thus with coordination number 12 for the two Zr-bricks (CN1=CN2=12), one or two linkers were removed making use of Zeobuilder [32]. In the category of species with one linker defect in the unit cell structure A, we select the two distinct configurations B and C as indicated in **Figure 2**.

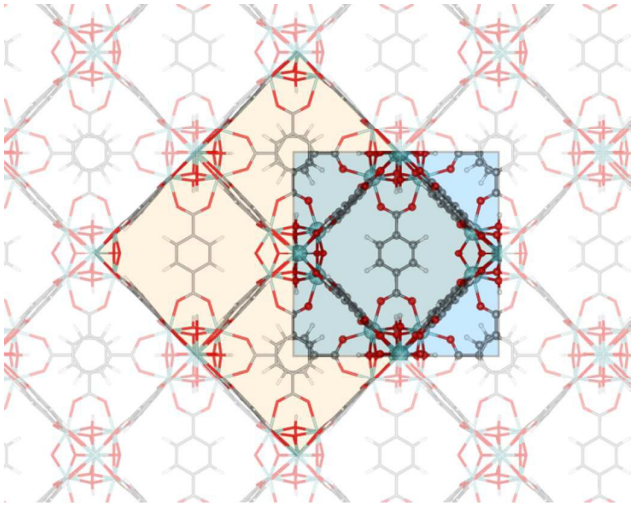

Figure 1 : Conventional unit cell of a defect free UiO-66 crystal with four Zr-bricks is indicated in orange. A reduced unit cell with only two Zr-bricks is shown in blue.

Within the concept of two Zr-bricks per unit cell, each brick is characterized by its coordination number CN1 and coordination number of its counterpart: $CN1^{CN2}$. For the convenience of the reader we display in **Figure 2** the two brick structures belonging to each configuration. The defect free configuration is composed of two 12^{12} bricks (or A0), the structure with one linker defect has two configurations $\{10^{12}, 12^{10}\}$ and $\{11^{11}, 11^{11}\}$ corresponding to the B and C structures shown in **Figure 2**. The index 0 is used to indicate that no dihydroxylation reaction has taken place yet. We limit the number of structurally different configurations with two linker defects within the picture of two Zr bricks per unit cell to three (labelled D, E and F); they belong to the family $\{10^{10}, 10^{10}\}$ and are displayed in **Figure 2**. Apparently knowledge of the coordination numbers of the two bricks in the unit cell is not sufficient to determine the defect structure uniquely. D0, E0 and F0 bricks clearly correspond to topologically different defect structures . The case in which a linker is removed from configuration B has not been considered since that would create inorganic $Zr_6O_7(OH)$-bricks that may not undergo water removal reactions. In total six defect configurations are retained and their behavior under dehydroxylation and their impact on mechanical properties will be investigated.

B. Effect of terephthalate defects on the material stability

Static periodic DFT calculations have been performed for all structures displayed in **Figure 2**. The applied methodology is explained in the Computational Methods section. For each of the optimized structures A-F electronic energies, frequencies, free energies and bulk moduli have been computed. It is clear that a linker removal is thermodynamically not favorable: the required electronic energy amounts to 380 kJ/mol and is almost equal for any linker (Electronic energies for each of the defect structures are given in Table S1 of the ESI). Defect structures B and C are almost isoenergetic. The gain in entropy at finite temperature does not significantly depend on the position of the removed linker yielding overall reaction free energies of 213 kJ/mol and 223 kJ/mol, for linker defect structure B and C, respectively at 320 °C (**Table 1**).

The coordination of each brick in the one-linker defect structures B and C is indicated in **Figure 2**, with the individual coordination numbers of each Zr-atom as well. They determine the spatial structure of each inorganic brick. In defect structure B we expect an equal coordination 7 for four Zr-atoms as demonstrated in brick **B0(10^{12})**. However, a more stringent level of theory in the geometry optimization of B reveals the presence of two minima on the potential energy surface due to some internal dislocations. One of the μ^3-oxo oxygens (see **B0(10^{12})**) jumps to a position out-of-plane bridging two Zr-centers (see **B'0(10^{12})**), and leaving a vacancy in the original position of the oxygen. Static periodic calculations learn that the last configuration is more stable with about 20 kJ/mol in electronic energy. We examined if the existence of a local minimum beside a global minimum is not an artifact of the applied computational methodology. This is however not the case since for

View Article Online
DOI: 10.1039/C6CE01027J

CrystEngComm

ARTICLE

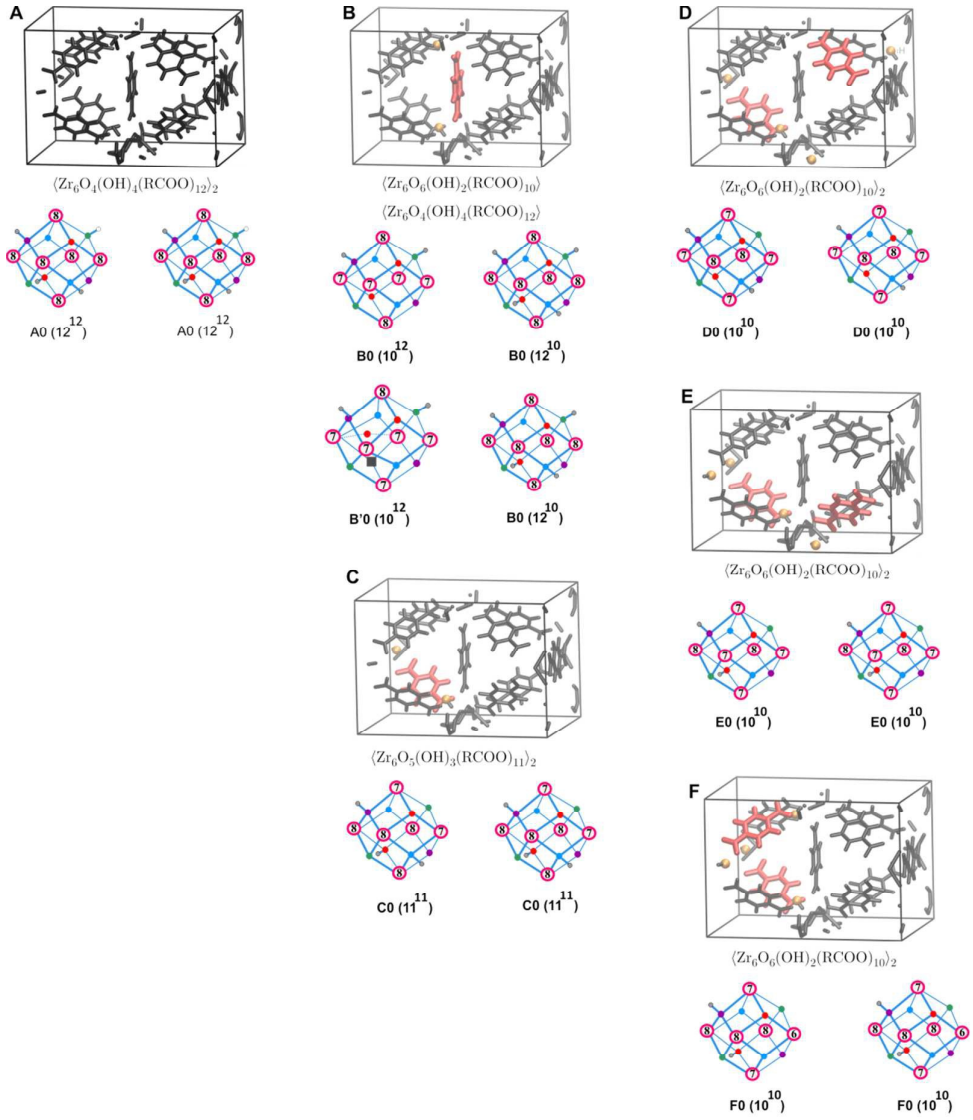

Figure 2 : The considered defect free and defect structures based on the unit cell with two Zr-bricks. Structure A corresponds to the structure without linker defect, B and C with structures bearing one linker defect and D, E and F with two linker defects. Coordination numbers of the two Zr-bricks in the unit cell are also given (CN_1 and CN_2). The removed terephthalate linkers are colored in red; furthermore they are displayed thicker to make their position visible in the unit cell. For convenience the notation $RCOO^-$ is introduced representing half a BDC^{2-} linker.

View Article Online
DOI: 10.1039/C6CE01027J

both defect configurations a distinct E(V) diagrams could be constructed, following the protocol given in the ESI.. As was recently shown by some of the presenting authors, geometry optimization of framework materials needs to be conducted with the greatest care which is furthermore confirmed here. [33] More computational details are taken up in the ESI. The E(V) curves are displayed in **Figure S.3**.

Removal of a second linker leading to structures of the type D, E or F (CN_1=10, CN_2=10) requires more or less the same free energy around ~ 210 kJ/mol at 320 °C (**Table 1**). Apparently, the free energy required to remove one linker does not depend very much whether already one linker was removed. The energy needed at 0 K to remove a terephthalate linker is of about 380 kJ/mol, which due to the entropy can be lowered to ~ 210 kJ/mol at a temperature of 320 °C. Experimentally a steady decrease of linker removal with increasing temperature and a full decomposition of the crystallinity at 450 °C was observed during TGA experiment of the group of Lillerud. [34] A complete overview of the free energy costs for linker removal at the six defect structures under study in this paper for different temperatures is given in Table S.1 of the ESI. Our calculations clearly show that the removal of linkers is an activated process, which does not spontaneously occur even at higher temperatures, which further confirms the stability of the material.

To assess the effect of missing terephthalate linkers in UiO-66 on the material stability, we varied the unit cell volume to construct an E(V) diagram and fitted the data points to a Birch-Murnagan equation of state (see ESI), from which we could deduce the bulk modulus. The bulk modulus is a measure for the compressibility of the periodic models, and we intuitively expect a decrease of this property with increasing amount of linker defects. This is indeed observed (see **Table 1**), as the bulk modulus decreases from 38 GPa for the ideal defect-free structure composed of inorganic $[Zr_6O_4(OH)_4]^{12+}$ bricks and terephthalate linkers forming a coordinatively saturated framework with eightfold coordination of Zr, to about 20 GPa on average for structures containing only $[Zr_6O_6(OH)_2]^{10+}$ bricks (shorthand notation 10^{10}). We notice a remarkable dependence of the bulk modulus on the position of the missing linker. The configuration B consisting of **B0(10^{12})** and **B0(12^{10})** bricks yields a bulk modulus of 31 GPa. The other category represented by configuration C (two **C0(11^{11})** bricks) delivers even a lower value (25 GPa). Removal of a second linker leads to a bulk modulus of about 21 GPa which is barely lower than the value corresponding with the one-linker defect structure C.

Compared with bulk moduli reported in literature, we notice a value of 41 GPa obtained by Wu et al. in a periodic PBE+D calculation for a defect-free UiO-66 material, comparable with our prediction of 38 GPa. Very recently, high-pressure PXRD experiments were carried out by Yot et al. [31] at different pressures p and at room temperature. From the evolution of the unit cell parameter as a function of p they deduced an experimental estimate for the bulk modulus of about 17 (± 1.5) GPa, which is

Table 1: Reaction free energies per unit cell of two Zr-bricks for the terephthalate linker removal and bulk modulus for each investigated structure. Free energy differences are given at 320 °C and a pressure of 1 bar with respect to the defect free structure **A**. For the energy balance a removed linker represented by terephthalic acid TA (H_2BDC) is treated in gas phase. $\Delta G = 1/x[G + x\ G_{TA} - G_A\ ]$ with x = number of removed linkers per unit cell. The results were obtained in a periodic calculation with the PBE-D3(BJ) level of theory, employing an energy cutoff of 600 eV. Bulk modulus was calculated from an E(V) fit to the Birch-Murnagan Equation of state. Experimental cell volume amounts to 4463 Å^3 [24] (scaled to the reduced unit cell of two Zr-bricks) for single crystals of UiO-66 with linker occupancy of 73 %.

	ΔG_{320} *(kJ/mol)*	Bulk modulus (GPa)	Volume of the optimized unit cell (Å^3)	Optimal volume from BM-fit (Å^3)
defect free structure (x=0)				
A. $<Zr_6O_4(OH)_4(RCOO)_{12}>_2$ $\{12^{12}, 12^{12}\}$	-	37.95	4540	4595
1 missing linker (x=1)				
B. $<Zr_6O_4(OH)_4(RCOO)_{12}>$ $<Zr_6O_6(OH)_2(RCOO)_{10}>$ $\{12^{10}, 10^{12}\}$	213.0	30.94	4512	4525
C. $<Zr_6O_5(OH)_3(RCOO)_{11}>$ $<Zr_6O_5(OH)_3(RCOO)_{11}>$ $\{11^{11}, 11^{11}\}$	222.9	24.66	4524	4553
2 missing linkers (x=2)				
D. $<Zr_6O_6(OH)_2(RCOO)_{10}>$ $<Zr_6O_6(OH)_2(RCOO)_{10}>$ $\{10^{10}, 10^{10}\}$	203.2	15.79	4573	4595
E. $<Zr_6O_6(OH)_2(RCOO)_{10}>$ $<Zr_6O_6(OH)_2(RCOO)_{10}>$ $\{10^{10}, 10^{10}\}$	226.1	21.25	4495	4525
F. $<Zr_6O_6(OH)_2(RCOO)_{10}>$ $<Zr_6O_6(OH)_2(RCOO)_{10}>$ $\{10^{10}, 10^{10}\}$	210.2	21.99	4509	4532

significantly lower than the DFT predictions of 41 GPa and 38 GPa. Thermogravimetric analyses (TGA) of their samples gave evidence for a small concentration of missing linkers (1 out of a total of 12) bringing our estimates of the bulk modulus obtained for 1 and 2 linker deficiencies much closer to the experiment. Anyway, the measured value is the highest reported so far for MOFs, emphasizing an extreme high-mechanical robustness for these Zr based MOFs, which further underlines the broad stability region of the UiO type materials regardless of the presence of defects (missing linkers and/or missing inorganic bricks).

C. Identifying Zr-O-Zr coordination by water after synthesis: a (de)hydration study

The stability of MOFs in a water environment is a crucial test for its further application within catalysis. A more extensive review on the nature of defects within catalysis has recently been presented by Farruseng et al.[35] UiO-66 frameworks are good candidates with respect to chemical and hydrothermal stability as was recently demonstrated by Leus et al. [4]

View Article Online
DOI: 10.1039/C6CE01027J

The identification and characterization of defects in MOFs on the molecular level remains a challenge and within this context the recent work of Lillerud and co-workers[24] and Yaghi and co-workers[26] can be considered as a milestone. With the extensive use of single-crystal X-ray diffraction (SXRD) missing linker defects in UiO-66 have been identified as water molecules coordinated directly to the Zr centers. Charge balancing as a result of the removal of linker(s) is achieved by an OH^- counterion, and hydrogen bonded as a μ^3-OH group to the pores of the inorganic Zr-brick. Inspired by that recent experimental work theoretical calculations have been performed focusing on the defect (Zr-O-Zr) coordination with water. To a large extent we elaborated on the original paper of Vandichel et al.[13] on defect creation in UiO-66. While in ref. [13] different linker replacements were taken into consideration during the synthesis process with BDC, TFA, HCl and H_2O in the reaction mixture, here focus lies on the different configurations of water coordination with the open metal site and the hydroxide counter ion replacing the negatively charged BDC linker. Very recently Ling and Slater [27] reported a computational study, where they reported the electronic energies for various water configurations based on static first principles approaches and studied the dynamics of the coordinating water molecules by means of ab initio molecular dynamics studies. Our approach may be regarded complementary as all our conclusions are based on periodic Density Functional Theory calculations and include all thermal corrections, which allows us to report free energies.

Periodic calculations DFT calculations were performed to determine the free energy of formation of different configurations with 3 defect coordinating water molecules (see Computational Methods). In order to be able to make a comparison with recent material published in the literature regarding this issue, we also investigate the case of one linker defect in the conventional unit cell consisting of four bricks as presented in **Figure 1**. Due to the symmetry of the defect-free material all one-linker defect structures within the representation of the conventional unit cell are equivalent. The reference configuration A represents the defect free site involving the BDC linker. If we follow the same notation as used in ref.[13], then A = X(BDC). Linker removal leads to configuration G (= X(0)) consisting of four Zr-bricks in the unit cell with coordination CN1=11, CN2=11, CN3=12 and CN4=12. It does not represent one of the one-linker structures B or C in **Figure 2** as this structure cannot be generated in the reduced unit cell of two bricks. A free energy of about 289 kJ/mol at synthesis conditions (T = 130 °C, p = 1 bar) is required to remove the linker from A. The coordination of water molecules near the defective site can occur in multiple configurations. Some of them are schematically displayed in **Figure 3a** considering three coordinating water molecules coordinated to each of the Zr atoms involved in the removal of one linker.

Physisorption of three water molecules onto one defect site results in a coordination free energy of about 68 kJ/mol (difference in energy between structure G and G_3H_2O). However after geometry optimization this structure quickly reorganizes into a state where the hydroxide anion is attached to the Zr atom and the oxo atom is protonated whereas the two other water molecules remain physisorbed. This configuration – labelled H-G_OH_2H_2O in **Figure 3a** – is even more stabilized with some extra 30 kJ/mol per brick (2 x 30 kJ/mol for the whole defect structure). The protonation of the other remaining μ^3 oxo-oxygen is less probable demanding some 80 kJ/mol (2 x 80 kJ/mol for the whole defect structure) to convert species H-G_OH_2H_2O to H_2-G_OH_OH_H_2O at synthesis conditions.

In a recent experimental paper, Trickett et al.[26] postulated the presence of a hydroxide anion originating from deprotonated atmospheric water coordinated to two water molecules after exposure of the defect site to the atmosphere and hydrogen bonding to the μ^3-OH groups of the metal cluster. The two schemes of **Figure 3** form an ideal platform to compare the theoretical results with the experimental findings of ref. [26] . As already mentioned before, we observed that during the geometry optimization of the structure G_3H_2O (empty defect site G with three water molecules) one of the water molecules undergoes a deprotonation with a proton transfer to an μ^3-oxo group of the Zr-brick inducing an μ^3-hydroxy group and the counterion OH^-, forming an intermediate hydroxide anion stabilized by three hydrogen bridges with two water molecules and the Zr-OH-Zr site. The position of the counterion OH^- is more or less bivalent. It can be coordinated with the metal Zr_1 as visualized in **Figure 4b**, or hydrogen bonded with the μ^3-hydroxy group as in **Figure 4a**. The left structure (**Figure 4a**) corresponds to the configuration proposed by Tricket et al. Our static periodic calculations predict the right structure (**Figure 4b**) to be more stable as was also found by Ling and Slater. Structure H-G_OH_2H_2O as visualized in **Figure 4b**, is energetically by far the most stable (gain in free energy of about 130 kJ/mol at synthesis conditions) as indicated in **Figure 3a.** Our static periodic results completely agree with the conclusions made by Ling and Slater, where the structure displayed in **Figure 4a** (labeled D3 in ref. [27]) is also found to be 155 kJ/mol less bound per defect center at 0 K. So, the structure postulated by Trickett et al. with a hydroxide anion hydrogen bonded to the μ^3-OH group of the metal cluster forms an intermediate configuration, which transforms to a defect site of structure H-G_OH_2H_2O as visualized in **Figure 4b**.

Summarizing, it is the position of the proton H_1 (indicated in **Figure 4**) that determines the molecular level characterization of the defect site. The structure postulated by Trickett et al. is not visible on the free energy surface of **Figure 3b** but only observed as a shallow intermediate. As the SXRD study of Trickett et al. reports relevant distances between oxygen atoms around the defect site, we also determine these distances in the optimized structure H-G_OH_2H_2O. These geometrical features may form an additional source of information regarding the true molecular structure of water coordination on the defect site. Relevant distances are those between the Zr-metal and oxygen of the hydroxyl anion and of the coordinated water molecule. Static periodic calculations yield values of 2.12 Å and 2.31 Å respectively for the Zr_1-O_1 and Zr_2-O_2 distances (**Figure 4b**) and thus valid for 0 K, while the values reported in the SXRD study correspond with various conditions of

View Article Online
DOI: 10.1039/C6CE01027J

CrystEngComm

ARTICLE

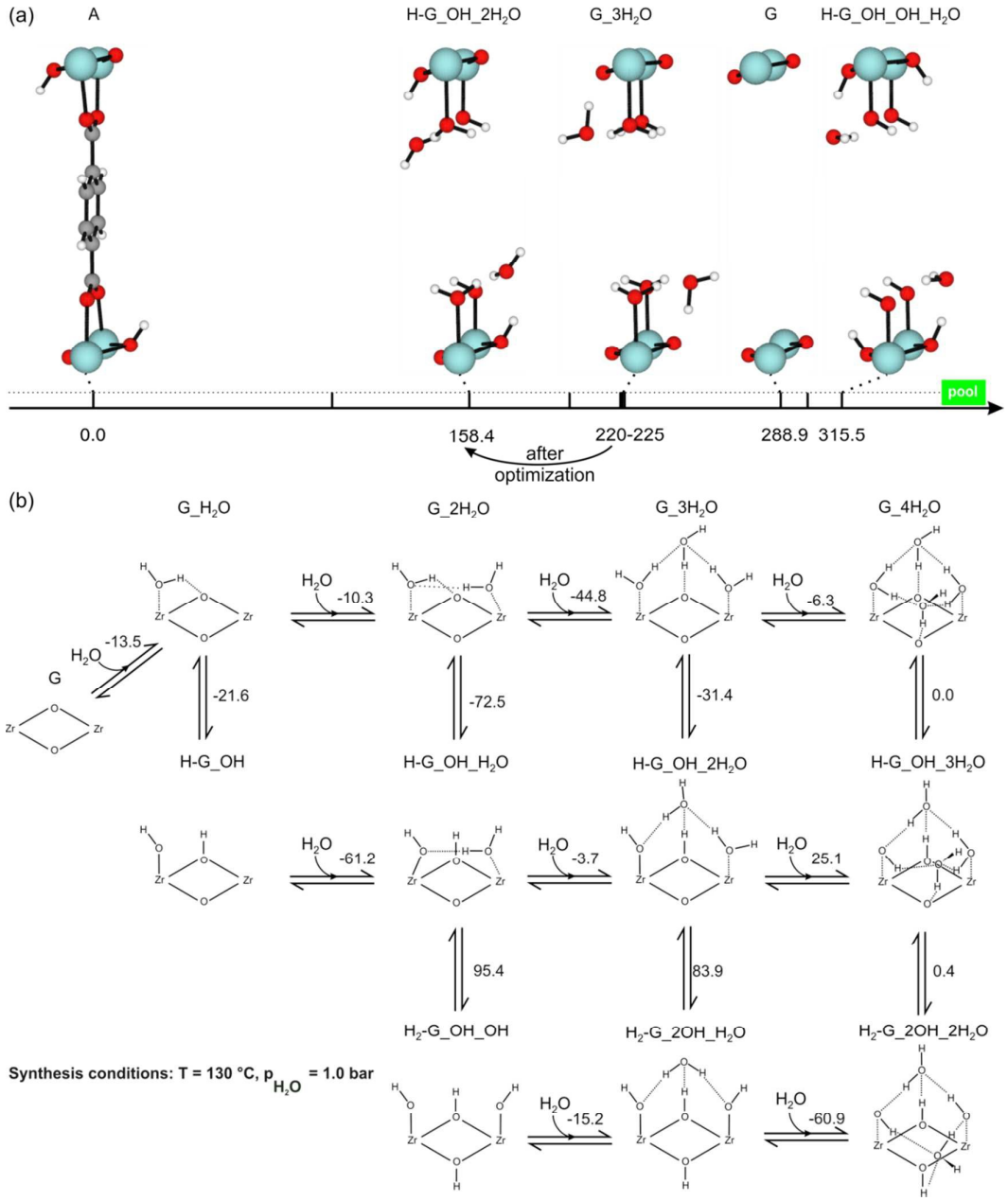

Figure 3a-b: (a) BDC incorporation compared with different coordination possibilities of 3 H_2O molecules during the synthesis of UiO-66. Free energy differences in kJ mol^{-1} are reported at synthesis conditions (T = 130 °C, p_{H2O} = 1 bar) with respect to the reference configuration A. A pool with isolated linkers and modulators in gas phase is added to guarantee mass balance in the equilibrium reactions. The results were obtained in a periodic calculation with the PBE-D3(BJ) functional, employing an energy cut-off of 600 eV; (b) Gibbs free energy diagram of water coordinating to defect sites, modeled on an extended cluster model of the UiO-66 at the B3LYP/[6-311++g(d,p),LanL2TZ(f)]//B3LYP/[6-31g(d),LanL2DZ] level of theory. Water molecules are approximated in gas phase; this approximation is

View Article Online
DOI: 10.1039/C6CE01027J

reasonable and makes a relative comparison between the different states possible. Free energies (in kJ/mol) for the different steps in the diagram are given at synthesis conditions.

temperature and pressure. Therefore, we complemented the static calculations with NVT molecular dynamic simulations to account for the temperature and to better explore the flat free energy surface comprising the defect site and the three coordinating water molecules. For details of the MD simulations we refer to the ESI. The system resides most of the time in a H-G_OH_2H_2O configuration during the simulations. The average distance of the hydroxide anion with the Zr atom (Zr-OH) amounts to 2.17 Å, while 2.40 Å on average for the distance between the metal and the coordinating water during the simulation (Zr-OH_2). Summarizing, the MD simulations predict Zr-O distances at room temperature that are slightly larger than the static estimates. The experimentally measured distances are on average: 2.24 Å for Zr-O and 2.73 Å for O4-O3 being the distance between the μ^3-hydroxy group and the oxygen of the coordinating water or OH^- counterion, as shown in **Figure 4**. When confronting the experimental ranges with the theoretical distances displayed in **Figure 4**, there is a clear preference to assign the structure H-G_OH_2H_2O as the best suited. The O4-O3 distance is the most decisive in this assignment. The hydroxyl anion in the case of the intermediate structure is stronger hydrogen bond to the μ^3-hydroxy group reproducing a O4-O3 distance of 2.51 Å which lies outside the experimental range. On the other hand on basis of the Zr-O distance the discrimination between the two configurations is less firm, as the Zr-O distances of the two pictures fit within the experimental range. The Zr-O distance is thus not a distinctive criterion to investigate the postulation of Trickett et al. To have even more convincing evidence for this, we also performed a MD simulation starting from 3 water molecules loosely adsorbed on a Zr-O-Zr defect site. This simulation could also shed light whether the two configurations of **Figure 4** have been visited during the simulation. Starting from the G_3H_2O state, the system was first equilibrated during 5 ps (10000 steps), and from that point the Zr1-O1 and Zr2-O2 distances were monitored for 10 ps (see **Figure 4** for the labeling of the atoms). During this simulation, we noticed quick proton jumps between Zr-OH_2 and Zr-OH species (**Figure S.1**, ESI), alternating between different states of the H-G_OH_2H_2O configuration via intermediate structures shown in **Figure 4a**. This intermediate structure (**Figure 4a**) as postulated by Trickett et al. is thus very shortlived as almost immediately the proton returned to an original H_G-OH_2H_2O configuration. Strikingly, the maximum in the distribution of O3-O4 (between 2.70 and 2.76 Å, **Figure S.2**) agrees with the experimentally obtained value of about 2.73 Å. All distances reported here in the above discussion on the structures displayed in **Figure 4** are fully consistent with those found by Ling and Slater.

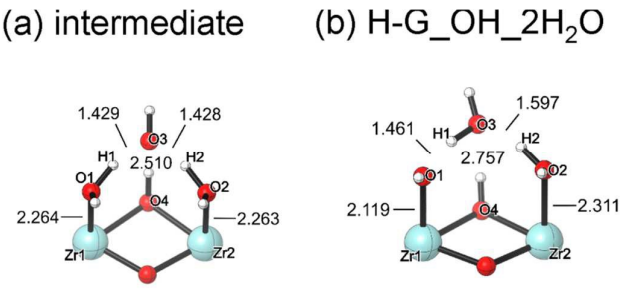

Figure 4: oxygen distances for (a) the defect site with three coordinating water molecules (b) anionic intermediate state during optimization of G_3H_2O and species H-G_OH_2H_2O. Both structures are optimized in a periodic model.

To assess the influence of the number of water molecules on the stability of various proposed structures, we also performed a series of cluster calculations in which a systematically increasing number of water molecules is added. For this purpose we used extended cluster calculations for the sake of computational efficiency. The results confirm what was found periodically, water is first physisorbed and then the structure quickly rearranges to a configuration corresponding to structure displayed in **Figure 4b**. The overall scheme of water coordination possibilities on the defect site is taken up in **Figure 3b**. Reaction free energies have been reported at synthesis conditions (T=130 °C and p_{H2O} = 1 bar). The changes of the reaction free energies resulting from different conditions of temperature and pressure are shown in Figure S.6 of the ESI. This free energy landscape unambiguously leads to H-G_OH_2H_2O and H-G_OH_H_2O as energetically most favorable configurations at atmospheric conditions. At synthesis conditions, the step from G to H-G_OH gives an overall free energy difference of -35 kJ/mol. This information can also be extracted from the periodic PBE-D3 calculations in ref.[13] where X(2H_2O) is favored over X(0) by about 60 kJ/mol, which is roughly the double of 30 kJ/mol and corresponds thus fairly well with the extended cluster calculations at B3LYP-D3 level here presented. The same extended cluster model to simulate the active Zr-site was also used recently by the authors to investigate aldol condensation reactions[12]. Structures with one hydroxyl group and some water molecules adsorbed **(structure** H-G_OH_xH_2O) seem to be the most favorable configurations regardless of the conditions of temperature and pressure. Based on energetic grounds configurations with one or two coordinated water molecules (H-G_OH_H_2O or H-G_OH_2H_2O) are the most abundant. However, if the vacuum is very strong (10^{-6} bar), there is a tendency to favor the coordination of only one water molecule (see free energy diagram of **Figure S.6**).

View Article Online
DOI: 10.1039/C6CE01027J

D. Dehydration reactions

A mechanistic proposal for the dehydration process of an inorganic brick of the UiO-66 material has been outlined in the previous paper of the authors on defect structures in UiO-66.[13] The electronic energy profile obtained after performance of a series of Nudged Elastic Band (NEB) simulations between initial and end structure reveals the appearance of two transition state structures. TS1 corresponds to a structure in which one carboxylic group is partially decoordinated from the Zr atom and in which the hydroxyl group is also detached from the Zr atom. This transition state is visualized in **Figure 5a** for the first dehydration reaction of the fully coordinated Zr-brick in a defect-free UiO-66 material. The second transition state TS2 corresponds with the protonation reaction of the released hydroxyl by abstraction of a proton of another available μ^3-OH group as visualized in **Figure 5b**. In this study we investigated systematically all dehydration processes starting from the six configurations A to F of **Figure 2** or **Table 1** representing the UiO-material with 0, 1 and two linker defects. An overview of the different dehydroxylation processes, taking place in the Zr-bricks belonging to the 6 UiO-66 structures under study in this work, is schematically shown in **Figure 6**. Pathway **A0 → A1** describes the first dehydroxylation of the defect-free $[Zr_6O_4(OH)_4]^{12+}$ brick. Coordination numbers of the different Zr-atoms in the brick are given (encircled). The initial structure **A0** (or 12^{12}) has coordination 8 for each Zr-atom in the brick. After removal of one water molecule, the brick reduces to $[Zr_6O_5(OH)_2]^{12+}$ with an oxygen vacancy displayed as a grey square in the second brick of the first row in **Figure 6**. The removal of a second water molecule leads to $[Zr_6O_6]^{12+}$, after which no further dehydration can take place. There are now two neighboring oxygen defects. In addition to the dehydroxylation scheme taken up in ref.[13], we now also report the free energy barriers of the two transition states TS1 and TS2 for each pathway and the reaction free energy. We performed these calculations for the six initial structures resulting to 9 water removal reactions in total. In addition 2 oxygen transfer reactions are also investigated (**Figure 6**). All local minima during the dehydration pathways and all transition states are further optimized employing a stronger convergence criterion for the electronic self-consistent field (SCF) problem. All free energies reported in **Figure 6** are evaluated at activation conditions (T = 320 °C, p = 10^{-6} bar) and they all give evidence to water removal on thermodynamical grounds, with reaction free energy differences ranging between -70 and -110 kJ/mol (**Figure 6**). For all CN=12 bricks (12-fold coordinated with terephthalate), the second dehydration reaction is higher activated than the first dehydration. To illustrate this, the first dehydroxylation on structure **A** exhibits barriers of 121.3 and 178.7 kJ/mol, while 171.7 and 212.4 kJ/mol for the second dehydroxylation (**Figure 6**). The free energy barriers for the second transition (**TS2**) may probably be slightly overestimated due to neglect of hydrogen tunneling effects. However, these corrections will not alter the general conclusions that we have drawn.

On the other hand, if an inorganic brick has two terephthalate deficiencies (i.e. $[Zr_6O_6(OH)_2]^{10+}$ or 10^{10}) the decoordination of the hydroxyl groups seems easier. Indeed, TS1 is much lower activated with barriers below 100 kJ/mol. This is in agreement with the lower bulk moduli for structures **D**, **E** and **F** that is representative for a lower compressibility, and thus increased global flexibility (see **Table 1**).

To investigate whether the dehydroxylation behavior of a $[Zr_6O_4(OH)_4]^{12+}$ brick is affected by the presence of neighboring linker deficiencies, a comparison between the dehydroxylation reactions of structure **A** (containing no terephthalate defect) and structure **B** (containing one terephthalate defect) learns that the latter predicts a slightly lower energy barrier for the first dehydroxylation (~15 kJ/mol) (compare pathway **A0 → A1** with **B0(12^{10}) → B1(12^{10})**) but that the barrier for the second dehydroxylation reaction varies even more substantially (~ 35 kJ/mol) (compare pathway **A1 → A2** with **B1(12^{10}) → B2(12^{10})**). It is thus expected that water removal becomes easier if there are even more neighboring linker deficiencies present. Indeed, in case of structures **D**, **E** and **F**, where all inorganic bricks have linker deficiencies, the activation barriers are lower than 156 kJ/mol confirming this hypothesis (**Figure 6**).

The evolution of the bulk modulus was calculated along all reaction paths in the harmonic limit (see ESI Sec. 2.1). The periodicity of the models means that dehydration occurs in every cell of the infinite periodic expansion, which makes the data not fully comparable with experiment where only some of the unit cells have linker defects. Energetic predictions are less sensitive to this periodicity effect, as was observed in the free energy of linker removal in **Table 1**. Nevertheless, the bulk modulus provides initial insight in the structural stability during the dehydration process.

The resistance against volume change under isotropic stress is best described by the Reuss bulk modulus B_R, which is computed from the inverse of the elastic tensor C. Similarly, the Reuss shear modulus G_R expresses the resistance to unit cell shape deformations. The observed trend in **Figure 7** is that linker removal weakens the structure, as already observed in Table 1. Dehydration further weakens the mechanical stability of UiO-66, but linker removal has a larger effect on the moduli than on the dehydroxylation steps. The moduli were also calculated for some other intermediate structures of the pathways, with occasionally a sudden drop in stiffness for structures close to transition states in the dehydroxylation pathways (data not shown). The reader should be warned that bulk moduli calculations are numerically sensitive and should be performed with caution. [33]

Comparison between bulk and shear modulus (**Figure 7**) shows that the UiO-66 is less resistant to shear than to isotropic pressure, meaning that the structure would deform considerably by pushing it sideways. However, with a shear modulus of about 17 GPa the Zr-MOF remains a material with an exceptional mechanical stability, which has also been observed by Wu et al. [25] reporting a minimal shear modulus of 13.7 GPa. These values correspond with fully

View Article Online
DOI: 10.1039/C6CE01027J

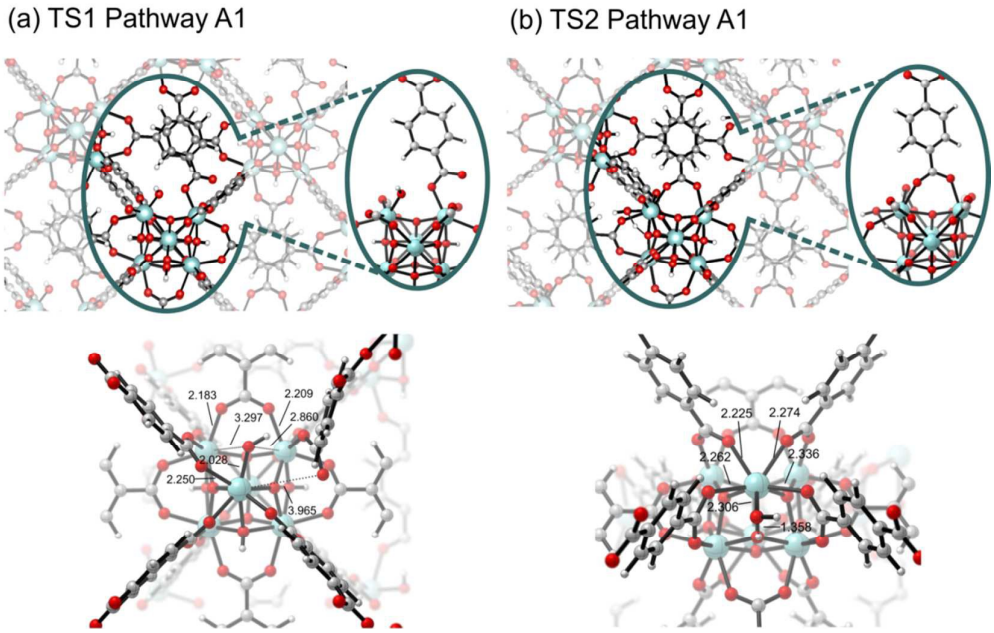

Figure 5: Visualization of the transition states TS1 and TS2 for the first dehydroxylation reaction A0 → A1 of $[Zr_6O_4(OH)_4]^{12+}$ (or 12^{12}) in a defect-free fully coordinated UiO-66 material at different view angles.

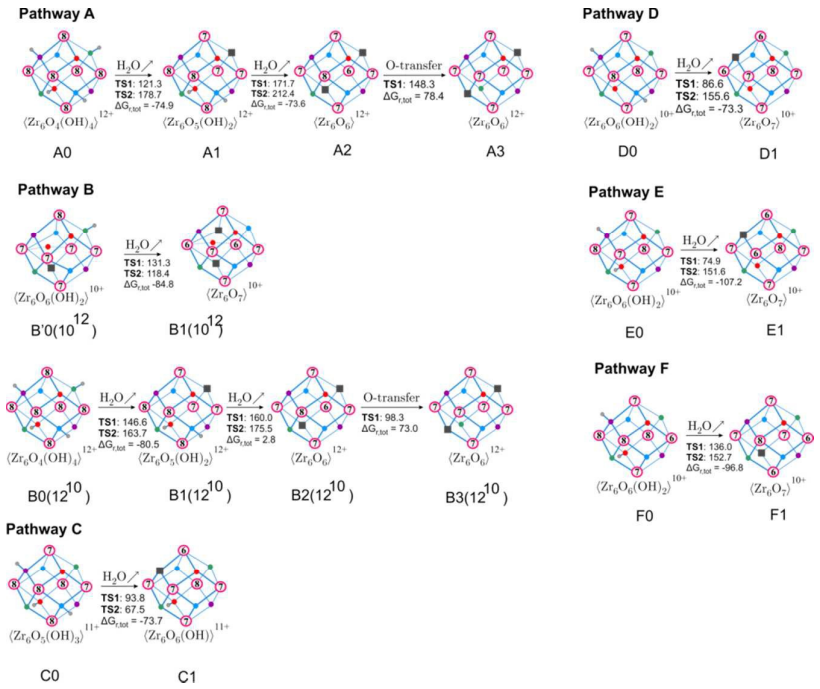

Figure 6: Schematic representation of the modeled dehydration reactions. The nomenclature of the different pathways A, B, C, D, E and F relies to their respective structures as defined in **Figure 2** and **Table 1**. Free energy barriers and reaction free energies in kJ mol^{-1} are reported at activation conditions (T = 320 °C, p = 10^{-6} bar). TS1 represents the barrier for terephthalate and hydroxyl decoordination, while TS2 represents the barrier for protonation of the hydroxyl group. The results were obtained in a periodic calculation with the PBE-D3(BJ) functional, employing an energy cutoff of 600 eV. ‡

View Article Online
DOI: 10.1039/C6CE01027J

CrystEngComm

ARTICLE

hydroxylated UiO-66. We also investigated the effect of dehydration on the shear modulus, and observed a steady decrease of this mechanical property. But with a shear modulus of 15 GPa, the dehydroxylated MOF still remains very robust under strain stress. The situation differs substantially when the material suffers from linker deficiencies. With two linkers missing the shear modulus drops down to 5 GPa , as clearly demonstrated in **Figure 7** (structure D). It strengthens the argument that the high Zr-O coordination and the high metal center to organic unit coordination lies on the basis of this exceptional strong resistance under strain stress, approaching that of zeolites. It should be noted that if only a few unit cells suffer from a linker defect, rather than each unit cell in the infinite periodic extension, the observed experimental bulk modulus will likely still resemble that of the structure without linker defects, as neighboring unit cells can still give stiffness to the crystal. More detailed bulk modulus profiles for all pathways are given in Section 4.4 of the ESI.

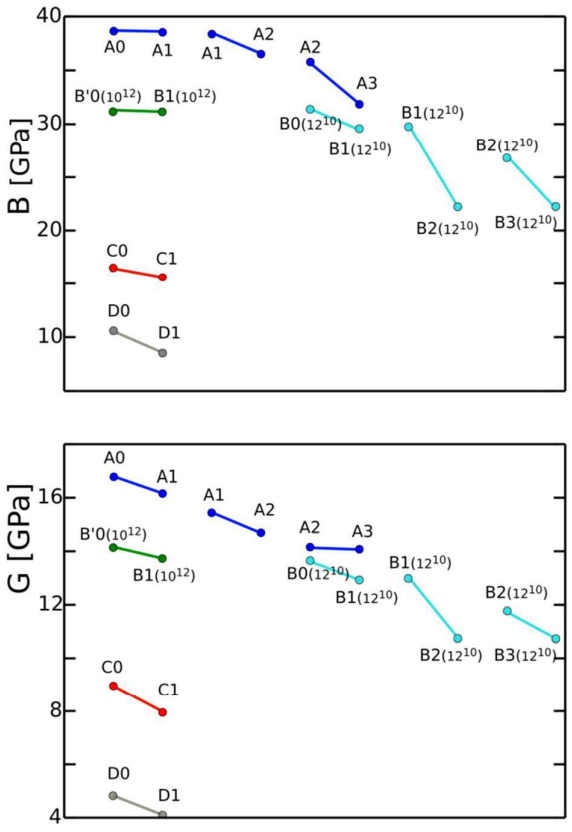

Figure 7a-b: Evolution of (a) the bulk modulus B_R and (b) shear modulus G_R along the reaction pathways

Oxygen transfer reactions

Oxygen transfers within Zr-bricks whereby a μ^3-oxygen jumps from its position to a vacancy belonging to the same inorganic brick are interesting processes as they determine the coordination degree of the Zr-atoms within an inorganic brick. Evidently, an oxygen transfer can only occur if an oxygen vacancy is present in the same Zr-brick. Some oxygen transfer reactions are taken up in the scheme of **Figure 6**. They start from a dehydrated inorganic brick with already two vacancies. The two oxygen transfer reactions taken up in the scheme all start from a completely dehydrated $[Zr_6O_6]^{12+}$ brick resulting after two subsequent dehydrations of a 12-fold coordinated $[Zr_6O_4(OH)_4]^{12+}$ brick (**pathways A2 → A3** and **B2(12^{10}) → B3(12^{10})**). The six Zr-atoms show a different coordination number. With an oxygen transfer reaction, all Zr atoms would become 7 fold coordinated – obtaining the coordination that has been postulated experimentally by Valenzano et al.[36]. However, with reaction free energies of more than 70 kJ/mol (320 ºC) such an oxygen transfer reaction is thermodynamically unfavorable. We also notice a slight decrease of the bulk modulus. Summarizing, within a dehydroxylated UiO-66 framework (without linker defects), we will most probably have a mixed Zr-coordination, with one Zr-atom that is six fold coordinated that has two oxygen vacancy sites as neighbors. The occurrence of a fully dehydrated Zr-brick with equal coordination numbers is less probable.

Experimental indications of dangling OH-groups during dehydroxylation processes

In this paper, we have postulated the dehydration as a two-step process with two transition states (TS1 and TS2). As the reaction barrier for the second step (water formation, TS2) is in most of the studied cases higher activated than for the first step (decoordination of a linker, TS1), we can expect that the intermediate dangling OH-groups are not so short-lived and should be observed in an in situ IR experiment were the temperature is gradually increased. Such experiment was already published by Lillerud et al.[37], and showed the presence of extra bands appearing at 3600-3700 cm^{-1}. The position of the dangling OH-group in the intermediate state between TS1 and TS2 is nicely visualized in step 20 of the reaction profile displayed in Figure 4 of ref. [13] . We constructed an extended cluster representing this intermediate state in pathway B0(10^{12}) → B1(10^{12}) and submitted it to a geometry optimization (**Figure 8**). An ab initio IR spectrum of a dangling OH-bond cluster demonstrates that the stretch vibration

View Article Online
DOI: 10.1039/C6CE01027J

of an OH dangling bond shifts to lower wavenumbers, exactly what was observed experimentally during a TG-DSC experiment. In near future, we can foresee the determination of an optimal activation temperature creating most dangling OH groups within UiO-66 type structures, and forming possible anchor points for ALD-precursors (ALD, atomic layer deposition) and coordinating homogeneous catalysts[38-40].

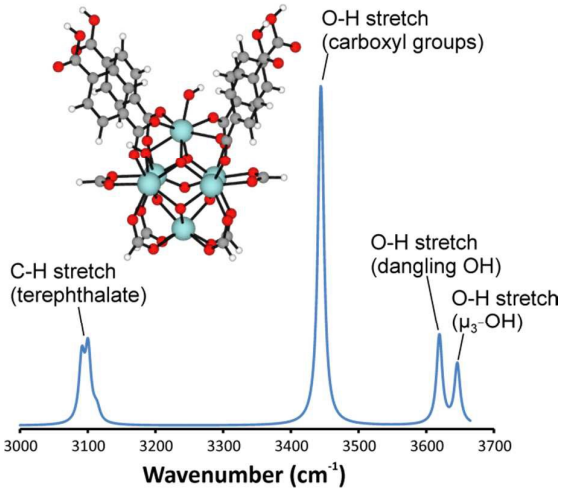

Figure 8: ab initio IR-spectra of a Zr-brick with a dangling OH-bond. Derived from a cluster model with level of theory B3LYP/(6-31g(d) + LanL2DZ). The ab initio spectrum was scaled with a factor 0.96.

Conclusions

In this paper an extensive characterization of the defect structures in the UiO-66 materials at the molecular level was presented. For this purpose different defect structures were constructed differing in the number of removed linkers and their position in the material. Each of the structures was characterized in terms of its energetic and mechanical stability, the degree of water coordination and the easiness to which water may be removed with dehydration reactions.

Following concluding remarks can be made:

i. Irrespective of the position of the linker, its removal costs a free energy of about 220 kJ/mol at atmospheric conditions and a temperature of 320 °C. The formation of missing linker vacancies after synthesis is thus unlikely due to the high energy required for the metal-ligand bond breaking and the removal of a linker may be regarded as an activated process.

ii. Pristine defect-free UiO-66 shows a mechanical robustness with a bulk modulus of 38 GPa which is extremely high and among the highest reported MOFs so far. Linker deficiencies lower the bulk modulus to values of about 20 GPa for UiO-66 crystals with a ten-fold coordination with the terephthalate linkers, but the material remains of an extraordinary stability.

iii. Linker deficiencies may cause a distortion of the metal-oxide nodes. Removal of the terephthalate linker (diagonal connecting two Zr-bricks in the reduced (blue) unit cell) induces a jump of an μ^3-oxygen to a position bridging two Zr-centres out-of-plane and creating a vacancy in one of the oxygen positions of the Zr-O brick. This oxygen transfer causes a reshuffle of the Zr-O coordination numbers.

iv. Water stabilizes the Zr-O-Zr defect site in case of a missing organic terephthalate linker and prefers a configuration in which the charge balancing hydroxide anion is coordinated to one of the Zr atoms whereas a μ^3-OH group is formed. The other water molecules remain physisorbed to the complex and help to stabilize the overall defect configuration. These findings are in agreement with the results of Ling and Slater. The structural arrangement, proposed by Trickett et al., where the charge balancing hydroxide anion is stabilized by a hydrogen bond with a neighbouring μ^3-OH group while the two Zr-atoms at the missing linker defect site are coordinated with the other water molecules, is energetically less favoured. However Trickett et al. made their conclusions on basis of distances between the relevant atoms of the Zr-brick and the water molecules and the hydroxide anion. All these distances are fairly well reproduced by our calculations and those of Ling et al. Our conclusion is that these distances are not able to uniquely assign the energetically most favourable configuration.

v. Dehydration reactions for each of the proposed structures were studied. Per water removal trajectory, two transition states are found; one corresponding with terephthalate and hydroxyl decoordination, one corresponding with the protonation of the dangling hydroxyl group. Dehydroxylation reactions happen more easily if there are more terephthalate defects, also when linker defects are present in neighboring bricks this enhances the water removal processes. Zr in a linker defect-free and dehydroxylated UiO-66 sample is not necessarily always sevenfold coordinated.

vi. We also investigated the defect structures under isotropic and strain stress. Our results affirm that dehydroxylation barely affects the robustness of the material and that linker deficiencies have much more impact on the bulk modulus. The various UiO-66 materials also resist fairly well to strain stress. While the shear modulus is almost half of its corresponding bulk modulus, it still much higher than any other MOF. The shear modulus drops down with 1 GPa on the average after each water removal, which is not spectacular, and the material conserves even in the fully dehydroxylated configuration a remarkable mechanical resistance.

View Article Online
DOI: 10.1039/C6CE01027J

After the activation (and thus also dehydration) of UiO-66 materials by a heat treatment at a certain temperature, a variety of possible defects are expected. A molecular level characterization of such defect structures is extremely challenging both from experimental and theoretical point of view. This work together with the other recent literature that appeared on the topic, shows that a combined experimental and theoretical approach is necessary to reach this goal. The results obtained here provide a basis to investigate effects of other ligands (e.g. substituted terephthalates, biphenyl, bipyridine, etc.) and metal cations (Ti, Hf, Ce, etc.), within other UiO-66 type MOFs.

Computational Methods

A. Cluster calculations

For the water adsorption study an extended cluster model for the UiO-66 [12] has been applied for the evaluation of the Gibbs free energy diagram of water coordination to the defect sites at different values of temperature and partial pressure. All structures were fully optimized at the DFT level of theory using the B3LYP hybrid functional [41, 42] and the usage of the Gaussian09 package[43]. The double-zeta Pople basis set 6–31G(d) was used for all the atoms except for Zr, for which the LANL2DZ effective core potential and basis set was applied [44]. The frequencies were calculated at the same level of theory as the geometry optimizations and confirmed that all structures were either local minima on the potential energy surface or transition states. Afterwards the energies were refined by single point energy calculations at the B3LYP/[H, C, O: 6-311++g(d,p), Zr: LanL2TZ(f)] level of theory. Furthermore, also the van der Waals corrections as developed by Grimme were included [45]. More specifically, the dispersion corrections are calculated according to the third version of Grimme [46] with Becke-Jones damping[47]. For the calculation of the Gibbs free energies, we used procedures as implemented in our in-house developed software module TAMKIN [48].

B. Molecular Dynamics simulations of water coordination

To study the water coordination within the UiO-66 material, ab initio molecular dynamics (AIMD) simulations are performed by means of density functional theory (DFT) calculations in a fully periodic UiO-66 catalyst model bearing one linker defect with unit cell formula $[Zr_6O_5(OH)_3(RCOO)_{11}]_2[Zr_6O_4(OH)_4(RCOO)_{12}]_2$. The AIMD simulations were performed with the CP2K simulation package[49] with Gaussian Plane Wave basis sets (GPW)[50, 51]. The BLYP functional[42, 52] with inclusion of Grimme D3 dispersion corrections[46] was chosen in combination with the DZVP-GTH basis set[53] for oxygen, carbon and hydrogen and the double-zeta MOLOPT basis set[54] for zirconium (plane wave cut off of 320 Ry). During the MD simulation, the temperature (298 K) was controlled by a chain of five Nosé-Hoover thermostats[55]. The time step for integration of the equations of motion [42]was set to 0.5 fs. The system was first equilibrated for 5 ps, and the average distances during the water coordination were determined over the next 10 ps.

C. Periodic calculations

To study the water adsorption and dehydroxylation pathways of the Zr-bricks, periodic DFT-D calculations are performed with the Vienna Ab Initio Simulation Package (VASP 5.2.12)[56-59]. The unit cells of all structures (**Figure 1**) are first optimized with a plane wave kinetic energy cutoff of 600 eV, employing the PBE exchange-correlation functional[60, 61] with D3-dispersion corrections according to Grimme[46] including Becke-Jones damping[47] (PBE-D3(BJ)). The projector augmented wave approximation (PAW)[62] is used and Brillouin zone sampling is restricted to the Γ-point. A gaussian smearing[57] of 0.05 eV is applied to improve convergence. Additionally, the convergence criterion for the electronic self-consistent field (SCF) problem is set to 10^{-5} eV for cell optimizations. Furthermore, the energy cut off for normal mode calculations is maintained at 600 eV for the energy refinements and frequency calculations at the PBE-D3(BJ) level of theory.

D. Dehydroxylation pathways

The same two-step procedure as outlined in the previous paper of the authors [13] will be applied to unravel the mechanism of the dehydroxylation process. First molecular dynamics NPT simulations were performed on the various periodic models at increasing temperatures to reveal the intermediate structures along the reaction pathways corresponding with the water removal processes from the inorganic $[Zr_6O_4(OH)_4]^{12+}$ bricks. These structures are further cell-optimized by means of periodic PBE-D3(BJ) calculations. In a second step the minimum energy pathways between the intermediate structures could be determined with the Nudged Elastic Band (NEB)-method[63, 64]. In order to determine whether we obtained local minima or transition states along the reaction pathways, a Hessian vibrational analysis (VA) has been performed.[65]

E. Bulk modulus

For the six starting structures (**Figure 2**), the bulk modulus B is derived by fitting the curvature at the minimum of the energy-versus-volume curve E(V) (Elec. Supp. Info. S2.1). This approach was found to be very efficient to avoid the effects of the Pulay stress in the search of the structure optimization instead of applying the standard conjugate gradient optimizer.[66] This Pulay stress can be seen as a finite basis set effect that artificially pushes the structure to small volumes. The effect causes here up to 1% volume change, but the relative volume ordering of the B/C and the D/E/F structures is not affected. Alternatively, the bulk modulus may also be derived from the elastic (stiffness) tensor C, yielding harmonic predictions for the bulk modulus. The Reuss bulk modulus B_R describes the strain response to isotropic stress, while the Reuss shear modulus G_R describes the resistance against unit cell deformation caused by shear stress. More details about their computation may be found in ref.[66] and in the ESI (S.2.1 and S.4.4).

View Article Online
DOI: 10.1039/C6CE01027J

Acknowledgements

M.V. acknowledges funding from the Scientific Research-Foundation Flanders (FWO) for a postdoctoral fellowship. J.H. thanks the FWO for funding (project number 3G048612). We also acknowledge BELSPO in the frame of IAP-PAI P7/05. VVS acknowledges funding from the European Union's Horizon 2020 research and innovation programme (consolidator ERC grant agreement No 647755 – DYNPOR (2015-2020)). The computational resources and services used in this work were provided by VSC (Flemish Supercomputer Center), funded by the Hercules foundation and the Flemish Government – department EWI.

Notes and references

‡ For TS1 of pathway B1, an extra imaginary frequency was found that could not be projected out after several geometry perturbations. This frequency was replaced with an arbitrary value of 50 cm^{-1}.

1. A. Corma, H. Garcia and F. Xamena, *Chemical Reviews*, 2010, **110**, 4606-4655.
2. D. Farrusseng, S. Aguado and C. Pinel, *Angewandte Chemie-International Edition*, 2009, **48**, 7502-7513.
3. M. Yoon, R. Srirambalaji and K. Kim, *Chem Rev*, 2012, **112**, 1196-1231.
4. K. Leus, T. Bogaerts, J. De Decker, H. Depauw, K. Hendrickx, H. Vrielinck, V. Van Speybroeck and P. Van der Voort, *Microporous Mesoporous Mat.*, 2016, **226**, 110-116.
5. L. Alaerts, E. Seguin, H. Poelman, F. Thibault-Starzyk, P. A. Jacobs and D. E. De Vos, *Chem-Eur J*, 2006, **12**, 7353-7363.
6. L. Mitchell, B. Gonzalez-Santiago, J. P. S. Mowat, M. E. Gunn, P. Williamson, N. Acerbi, M. L. Clarke and P. A. Wright, *Catalysis Science & Technology*, 2013, **3**, 606-617.
7. Y. Fu, D. Sun, M. Qin, R. Huang and Z. Li, *Rsc Advances*, 2012, **2**, 3309-3314.
8. K. Leus, I. Muylaert, M. Vandichel, G. B. Marin, M. Waroquier, V. Van Speybroeck and P. Van der Voort, *Chemical Communications*, 2010, **46**, 5085-5087.
9. K. Leus, M. Vandichel, Y. Y. Liu, I. Muylaert, J. Musschoot, S. Pyl, H. Vrielinck, F. Callens, G. B. Marin, C. Detavernier, P. V. Wiper, Y. Z. Khimyak, M. Waroquier, V. Van Speybroeck and P. Van der Voort, *Journal of Catalysis*, 2012, **285**, 196-207.
10. F. Vermoortele, M. Vandichel, B. Van de Voorde, R. Ameloot, M. Waroquier, V. Van Speybroeck and D. E. De Vos, *Angew. Chem.-Int. Edit.*, 2012, **51**, 4887-4890.
11. M. Vandichel, S. Biswas, K. Leus, J. Paier, J. Sauer, T. Verstraelen, P. Van der Voort, M. Waroquier and V. Van Speybroeck, *Chempluschem*, 2014, **79**, 1183-1197.
12. J. Hajek, M. Vandichel, B. Van de Voorde, B. Bueken, D. De Vos, M. Waroquier and V. Van Speybroeck, *Journal of Catalysis*, 2015, **331**, 1-12.
13. M. Vandichel, J. Hajek, F. Vermoortele, M. Waroquier, D. E. De Vos and V. Van Speybroeck, *Crystengcomm*, 2015, **17**, 395-406.
14. U. Ravon, M. E. Domine, C. Gaudillere, A. Desmartin-Chomel and D. Farrusseng, *New J Chem*, 2008, **32**, 937-940.
15. U. Ravon, M. Savonnet, S. Aguado, M. E. Domine, E. Janneau and D. Farrusseng, *Micropor Mesopor Mat*, 2010, **129**, 319-329.
16. M. J. Cliffe, J. A. Hill, C. A. Murray, F. X. Coudert and A. L. Goodwin, *Phys. Chem. Chem. Phys.*, 2015, **17**, 11586-11592.
17. M. J. Cliffe, W. Wan, X. Zou, P. A. Chater, A. K. Kleppe, M. G. Tucker, H. Wilhelm, N. P. Funnell, F. X. Coudert and A. L. Goodwin, *Nature communications*, 2014, **5**, 4176.
18. F. Vermoortele, B. Bueken, G. Le Bars, B. Van de Voorde, M. Vandichel, K. Houthoofd, A. Vimont, M. Daturi, M. Waroquier, V. Van Speybroeck, C. Kirschhock and D. E. De Vos, *J Am Chem Soc*, 2013, **135**, 11465-11468.
19. J. H. Cavka, S. Jakobsen, U. Olsbye, N. Guillou, C. Lamberti, S. Bordiga and K. P. Lillerud, *Journal of the American Chemical Society*, 2008, **130**, 13850-13851.
20. D. S. Sholl and R. P. Lively, *The Journal of Physical Chemistry Letters*, 2015, DOI: 10.1021/acs.jpclett.5b01135, 3437-3444.
21. Z. L. Fang, B. Bueken, D. E. De Vos and R. A. Fischer, *Angew. Chem.-Int. Edit.*, 2015, **54**, 7234-7254.
22. M. D. Allendorf and V. Stavila, *Crystengcomm*, 2015, **17**, 229-246.
23. J. Canivet, M. Vandichel and D. Farrusseng, *Dalton Transactions*, 2016, **45**, 4090-4099.
24. S. Oien, D. Wragg, H. Reinsch, S. Svelle, S. Bordiga, C. Lamberti and K. P. Lillerud, *Cryst. Growth Des.*, 2014, **14**, 5370-5372.
25. H. Wu, T. Yildirim and W. Zhou, *Journal of Physical Chemistry Letters*, 2013, **4**, 925-930.
26. C. A. Trickett, K. J. Gagnon, S. Lee, F. Gandara, H.-B. Buergi and O. M. Yaghi, *Angewandte Chemie-International Edition*, 2015, **54**, 11162-11167.
27. S. Ling and B. Slater, *Chem. Sci.*, 2016, DOI: 10.1039/C5SC04953A, in press.
28. J. Li, P. Huang, X.-R. Wu, J. Tao, R.-B. Huang and L.-S. Zheng, *Chem. Sci.*, 2013, **4**, 3232-3238.
29. T. K. Pal, S. Neogi and P. K. Bharadwaj, *Chem.-Eur. J.*, 2015, **21**, 16083-16090.
30. R. Sen, D. Saha, S. Koner, P. Brandao and Z. Lin, *Chem.-Eur. J.*, 2015, **21**, 5962-5971.
31. P. G. Yot, K. Yang, F. Ragon, V. Dmitriev, T. Devic, P. Horcajada, C. Serre and G. Maurin, *Dalton Transactions*, 2016, **45**, 4283-4288.
32. T. Verstraelen, V. Van Speybroeck and M. Waroquier, *Journal of Chemical Information and Modeling*, 2008, **48**, 1530-1541.
33. D. E. P. Vanpoucke, K. Lejaeghere, V. Van Speybroeck, M. Waroquier and A. Ghysels, *J. Phys. Chem. C*, 2015, **119**, 23752-23766.
34. G. C. Shearer, S. Chavan, J. Ethiraj, J. G. Vitillo, S. Svelle, U. Olsbye, C. Lamberti, S. Bordiga and K. P. Lillerud, *Chem. Mat.*, 2014, **26**, 4068-4071.
35. J. Canivet, A. Fateeva, Y. M. Guo, B. Coasne and D. Farrusseng, *Chem Soc Rev*, 2014, **43**, 5594-5617.
36. L. Valenzano, B. Civalleri, S. Chavan, S. Bordiga, M. H. Nilsen, S. Jakobsen, K. P. Lillerud and C. Lamberti, *Chem Mater*, 2011, **23**, 1700-1718.
37. G. C. Shearer, S. Forselv, S. Chavan, S. Bordiga, K. Mathisen, M. Bjorgen, S. Svelle and K. P. Lillerud, *Topics in Catalysis*, 2013, **56**, 770-782.

View Article Online
DOI: 10.1039/C6CE01027J

38. D. Yang, S. O. Odoh, T. C. Wang, O. K. Farha, J. T. Hupp, C. J. Cramer, L. Gagliardi and B. C. Gates, *J Am Chem Soc*, 2015, **137**, 7391-7396.
39. I. S. Kim, J. Borycz, A. E. Platero-Prats, S. Tussupbayev, T. C. Wang, O. K. Farha, J. T. Hupp, L. Gagliardi, K. W. Chapman, C. J. Cramer and A. B. F. Martinson, *Chem Mater*, 2015, **27**, 4772-4778.
40. J. E. Mondloch, W. Bury, D. Fairen-Jimenez, S. Kwon, E. J. DeMarco, M. H. Weston, A. A. Sarjeant, S. T. Nguyen, P. C. Stair, R. Q. Snurr, O. K. Farha and J. T. Hupp, *J Am Chem Soc*, 2013, **135**, 10294-10297.
41. A. D. Becke, *Journal of Chemical Physics*, 1993, **98**, 5648-5652.
42. C. T. Lee, W. T. Yang and R. G. Parr, *Physical Review B*, 1988, **37**, 785-789.
43. R. A. Gaussian 09, Frisch, M. J.; Trucks, G. W.; Schlegel, H. B.; Scuseria, G. E.; Robb, M. A.; Cheeseman, J. R.; Scalmani, G.; Barone, V.; Mennucci, B.; Petersson, G. A.; Nakatsuji, H.; Caricato, M.; Li, X.; Hratchian, H. P.; Izmaylov, A. F.; Bloino, J.; Zheng, G.; Sonnenberg, J. L.; Hada, M.; Ehara, M.; Toyota, K.; Fukuda, R.; Hasegawa, J.; Ishida, M.; Nakajima, T.; Honda, Y.; Kitao, O.; Nakai, H.; Vreven, T.; Montgomery, Jr., J. A.; Peralta, J. E.; Ogliaro, F.; Bearpark, M.; Heyd, J. J.; Brothers, E.; Kudin, K. N.; Staroverov, V. N.; Kobayashi, R.; Normand, J.; Raghavachari, K.; Rendell, A.; Burant, J. C.; Iyengar, S. S.; Tomasi, J.; Cossi, M.; Rega, N.; Millam, J. M.; Klene, M.; Knox, J. E.; Cross, J. B.; Bakken, V.; Adamo, C.; Jaramillo, J.; Gomperts, R.; Stratmann, R. E.; Yazyev, O.; Austin, A. J.; Cammi, R.; Pomelli, C.; Ochterski, J. W.; Martin, R. L.; Morokuma, K.; Zakrzewski, V. G.; Voth, G. A.; Salvador, P.; Dannenberg, J. J.; Dapprich, S.; Daniels, A. D.; Farkas, Ö.; Foresman, J. B.; Ortiz, J. V.; Cioslowski, J.; Fox, D. J. Gaussian, Inc., Wallingford CT, 2009., unpublished work.
44. P. J. Hay and W. R. Wadt, *Journal of Chemical Physics*, 1985, **82**, 270-283.
45. S. Grimme, *Journal of Computational Chemistry*, 2004, **25**, 1463-1473.
46. S. Grimme, J. Antony, S. Ehrlich and H. Krieg, *Journal of Chemical Physics*, 2010, **132**.
47. S. Grimme, S. Ehrlich and L. Goerigk, *Journal of Computational Chemistry*, 2011, **32**, 1456-1465.
48. A. Ghysels, T. Verstraelen, K. Hemelsoet, M. Waroquier and V. Van Speybroeck, *J. Chem Inf. Model.*, 2010, **50**, 1736-1750.
49. J. VandeVondele, M. Krack, F. Mohamed, M. Parrinello, T. Chassaing and J. Hutter, *Computer Physics Communications*, 2005, **167**, 103-128.
50. G. Lippert, J. Hutter and M. Parrinello, *Theoretical Chemistry Accounts*, 1999, **103**, 124-140.
51. G. Lippert, J. Hutter and M. Parrinello, *Molecular Physics*, 1997, **92**, 477-487.
52. A. D. Becke, *Physical Review A*, 1988, **38**, 3098-3100.
53. S. Goedecker, M. Teter and J. Hutter, *Physical Review B*, 1996, **54**, 1703-1710.
54. J. VandeVondele and J. Hutter, *The Journal of Chemical Physics*, 2007, **127**, 114105.
55. D. Frenkel and B. Smit, in *Understanding Molecular Simulation (Second Edition)*, Academic Press, San Diego, 2002, DOI: http://dx.doi.org/10.1016/B978-012267351-1/50008-0, pp. 139-163.
56. G. Kresse and J. Furthmuller, *Physical Review B*, 1996, **54**, 11169-11186.
57. G. Kresse and J. Furthmuller, *Computational Materials Science*, 1996, **6**, 15-50.
58. G. Kresse and J. Hafner, *Physical Review B*, 1993, **47**, 558.
59. G. Kresse and J. Hafner, *Physical Review B*, 1994, **49**, 14251.
60. J. P. Perdew, K. Burke and M. Ernzerhof, *Physical Review Letters*, 1996, **77**, 3865.
61. J. P. Perdew, K. Burke and M. Ernzerhof, *Physical Review Letters*, 1997, **78**, 1396.
62. P. E. Blochl, *Physical Review B*, 1994, **50**, 17953-17979.
63. G. Mills, H. Jonsson and G. K. Schenter, *Surf Sci*, 1995, **324**, 305-337.
64. G. Henkelman, B. P. Uberuaga and H. Jónsson, *The Journal of Chemical Physics*, 2000, **113**, 9901-9904.
65. B. A. De Moor, A. Ghysels, M.-F. Reyniers, V. Van Speybroeck, M. Waroquier and G. B. Marin, *Journal of Chemical Theory and Computation*, 2011, **7**, 1090-1101.
66. D. E. P. Vanpoucke, K. Lejaeghere, V. Van Speybroeck, M. Waroquier and A. Ghysels, *The Journal of Physical Chemistry C*, 2015, **119**, 23752-23766.